J. Fluid Mech. (1979), *vol.* 93, *part* 2, *pp.* 379–400
Printed in Great Britain

Development of radiation fields and baroclinic eddies in a β-plane

By C. L. TANG

Bedford Institute of Oceanography, Dartmouth, N.S., Canada

(Received 9 November 1977 and in revised form 7 September 1978)

The evolution of an eddy in a two-layer shear flow and the radiation field generated by the eddy are investigated by solving the initial value problem. The solution indicates that two wave regimes with different characteristics exist in the $\mathbf{x}/t$ plane, where t is the time and $\mathbf{x}$ is the distance from the initial disturbance. The near-field (small $\mathbf{x}/t$) behaviour depends critically on the stability of the shear. In a baroclinically stable shear flow, the radiation field of the baroclinic waves is confined to a region the boundary of which expands linearly with time. If the shear flow is baroclinically unstable, the eddy gradually evolves from an isotropic structure into a wave packet that grows exponentially and expands as the square root of time. The far field (large $\mathbf{x}/t$) consists mainly of long barotropic Rossby waves. As $\mathbf{x}/t$ increases, the effect of the mean currents becomes weaker and the motion becomes increasingly barotropic in character. If we consider the strong boundary current as a source of baroclinic energy in the ocean, the far-field results show that the mid-ocean eddies can reach large amplitudes independent of the mean currents. The transient motion (small $\mathbf{x}$ and t) of the eddy is examined by numerically computing the stream function from the solution. The results show that the combined actions of baroclinic instability and wave dispersion cause an initially isotropic eddy to remain roughly isotropic for a relatively long period of time. This suggests that the initial development of unstable eddies cannot be neglected in studying the meridional scale of the eddy field in the atmosphere. Application of the model to study the dispersion of wind-generated Rossby waves is discussed.

1. Introduction

Instability has long been known to play an important role in the circulation and energy transfer in the atmosphere and the ocean. Baroclinic instability in particular has been investigated extensively since Charney's (1947) pioneering work on cyclone waves in the atmosphere. In the ocean, Gill, Green & Simmons (1974) have shown that there is sufficient potential energy available in the mean circulation which can be converted into eddy energy. They suggested baroclinic instability as the mechanism for such an energy conversion. Robinson & McWilliams (1974) have studied the properties of the unstable baroclinic waves in an ocean with a gentle bottom slope and vertical shears in arbitrary directions. These studies provide a framework for understanding the relationships between the mean shears and the eddies, but they were unsatisfactory in several respects.

The implicit assumption used in single wave analysis is that the observed eddies correspond to the fastest growing baroclinic waves. The validity of this assumption

0022–1120/79/4229–6950 $02.00

depends on the transient period, t_T, for the development of a single wave spectrum, and the time scale, t_N, of nonlinear interactions which distort a linear baroclinic wave field. The results of single wave analysis are valid only in the time range $t_T < t < t_N$ ($t = 0$ is the onset of the perturbation). If t_T and t_N are of the same order of magnitude, the usefulness of the single wave analysis is greatly restricted. Moreover, without a consideration of the initial development, the structure of young eddies ($t < t_T$) cannot be studied.

In this paper, we solve the initial value problem for a localized disturbance in a uniform two-layer zonal flow in a β-plane. By considering the entire time history of the perturbation, we extend the validity of the linear baroclinic instability theory to a time range $0 < t < t_N$. The results can be used to examine the following questions.

(*a*) The spatial scale of eddy field in a zonal shear flow. This problem has been investigated by many authors in the meteorology literature (for example, Moura & Stone 1976). Most of the studies examined the structure of unstable eddies in their fully developed stage (exponential growth). The small t ($t < t_N$) contributions, which may be significant in the equilibrium state, were not considered. The solution of an initial value problem will reveal the pattern of development from the onset of the perturbation to the fully developed stage.

(*b*) The spatial variation of eddy motions in the North Atlantic. Observations of temperature and salinity distributions (Lee Dantzler 1976, 1977) and results of numerical models (Semtner & Mintz 1977; Holland & Lin 1975) indicate that the baroclinic energy is strongest near the Gulf Stream, and decreases with increasing distance from it. This suggests production of eddies by baroclinic instability in the Gulf Stream region. The solution of an initial value problem allows us to study the motions both in the generation region (the near field) and in the ocean interior (the far field). While the uniform zonal mean shear used in this paper may not be a realistic representation of the shears in the North Atlantic, the question of whether the far-field solution can be applied to the ocean interior really depends on the sensitivity of the results. If the results for the far field are insensitive to the mean shear then a model with a variable mean shear would not give results greatly different from a model with a uniform mean shear.

(*c*) The response of a stratified shear flow to a localized wind system. The response of an ocean without mean currents has been investigated by Longuet-Higgins (1965). The problem we consider here is an extension of his work to include mean currents.

2. The governing equations

The geometry of the model is shown in figure 1. By using the geostrophic approximation to the vorticity and expanding the vorticity equations for each layer to first order in $(D_n - H_n)/H_n$, where D_n is the total thickness and H_n is the average thickness of layer n (Stern 1975), we obtain the equations for the stream functions, Ψ_1 and Ψ_2, of the two-layer quasi-geostrophic system:

$$\left(\frac{\partial}{\partial t}+\frac{\partial \Psi_1}{\partial x}\frac{\partial}{\partial y}-\frac{\partial \Psi_1}{\partial y}\frac{\partial}{\partial x}\right)[\nabla^2\Psi_1 - F_1(\Psi_1-\Psi_2)+\beta y] = 0, \tag{1a}$$

$$\left(\frac{\partial}{\partial t}+\frac{\partial \Psi_2}{\partial x}\frac{\partial}{\partial y}-\frac{\partial \Psi_2}{\partial y}\frac{\partial}{\partial x}\right)[\nabla^2\Psi_2 + F_2(\Psi_1-\Psi_2)+By] = 0, \tag{1b}$$

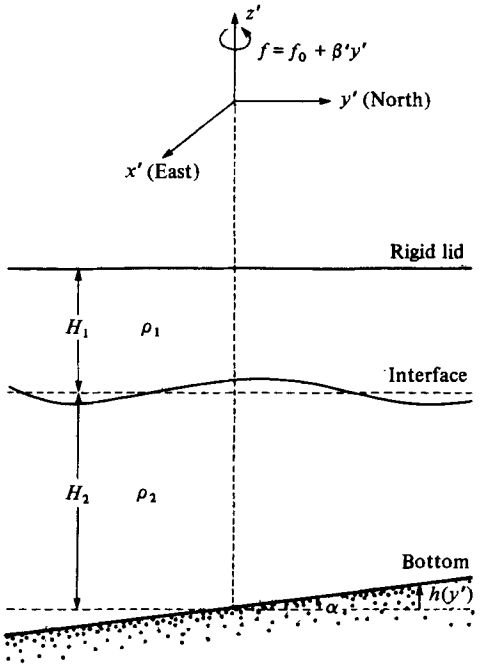

FIGURE 1. Geometry of the two-layer model.

where the subscripts 1 and 2 refer to the upper and the lower layers respectively. All the variables in (1*a*) and (1*b*) have been non-dimensionalized by a length scale L, a velocity scale U_0, and a time scale L/U_0. They are related to the dimensional variables (denoted by primes) by

$$(x', y') = L(x, y), \quad t' = (L/U_0)\,t, \quad \Psi'_n = \rho f_0 U_0 L \Psi_n,$$

$$\beta' = (U_0/L^2)\,\beta, \quad F'_n = L^{-2} F_n \quad \text{and} \quad B' = (U_0/L^2)\,B,$$

where F'_n and B' are defined by

$$F'_n = f_0^2/(g_r H_n) \quad \text{and} \quad B' = H_2 \frac{\partial}{\partial y'}\left(\frac{f(y')}{H_2 - h(y')}\right),$$

with

$$f(y') = f_0 + \beta' y' \quad \text{and} \quad g_r = g(\rho_2 - \rho_1)/\rho_1,$$

where $f(y')$ and g_r are the Coriolis parameter and the reduced gravity in dimensional units respectively, and $h(y')$ is the deviation of the sea bottom from the horizontal plane (see figure 1).

B is assumed constant. For a small bottom slope, $B = \beta + \alpha f_0 L^2/(U_0 H_2)$, where α is the inclination (see figure 1), and (1*a*) and (1*b*) become identical to the corresponding equations in Gill *et al.* (1974), Smith (1976), and Mysak & Schott (1977).

Let ψ_n be the perturbation to a basic pressure corresponding to a uniform geostrophic zonal current, U_n, i.e.

$$\Psi_n = -U_n y + \psi_n, \quad n = 1, 2. \tag{2}$$

Substituting (2) into (1a) and (1b) yields the linearized equations for ψ_n,

$$\left(\frac{\partial}{\partial t}+U_1\frac{\partial}{\partial x}\right)[\nabla^2\psi_1-F_1(\psi_1-\psi_2)]+[\beta+F_1(U_1-U_2)]\frac{\partial\psi_1}{\partial x}=0 \tag{3a}$$

and

$$\left(\frac{\partial}{\partial t}+U_2\frac{\partial}{\partial x}\right)[\nabla^2\psi_2+F_2(\psi_1-\psi_2)]+[B-F_2(U_1-U_2)]\frac{\partial\psi_2}{\partial x}=0. \tag{3b}$$

3. The initial value problem

Equations (3a) and (3b) define a unique solution for a given set of initial and boundary condition. We shall use the Fourier transform method to find the solution. Eliminating $\psi_1(\psi_2)$ from (3a) and (3b), we have the decoupled equation for $\psi_2(\psi_1)$:

$$\mathscr{L}(\mathbf{x},t)\,\psi_n(\mathbf{x},t)=0, \quad n=1,2, \tag{4}$$

where $\mathscr{L}(\mathbf{x},t)$ is a differential operator of second order in t and sixth order in $\mathbf{x}$. Its explicit form is given in appendix A. For a $\psi_n(\mathbf{x},t)$ that approaches zero sufficiently fast as $\mathbf{x}\to\infty$, we can define a Fourier transform with respect to $\mathbf{x}$ by

$$\overline{\psi}_n(\mathbf{k},t)=\frac{1}{(2\pi)^2}\int\psi_n(\mathbf{x},t)\exp(i\mathbf{k}.\mathbf{x})\,d\mathbf{x}, \quad n=1,2. \tag{5}$$

The equation for $\overline{\psi}_n(\mathbf{k},t)$ is

$$\overline{\mathscr{L}}(\mathbf{k},t)\,\overline{\psi}_n(\mathbf{k},t)=0, \quad n=1,2, \tag{6}$$

where

$$\overline{\mathscr{L}}(\mathbf{k},t)=\mathscr{L}(-i\mathbf{k},t).$$

Equation (6) can be written in the form

$$[a(\mathbf{k})\,\partial_t^2+b(\mathbf{k})\,\partial_t+c(\mathbf{k})]\,\overline{\psi}_n(\mathbf{k},t)=0, \quad n=1,2. \tag{7}$$

The solution of (7) is a linear combination of

$$\exp\{i[P(\mathbf{k})+Q(\mathbf{k})]t\} \quad \text{and} \quad \exp\{i[P(\mathbf{k})-Q(\mathbf{k})]t\},$$

where

$$\begin{aligned}P(\mathbf{k})&=-b(\mathbf{k})/2ia(\mathbf{k})\\&=\frac{k_x}{2k^2(k^2+F_1+F_2)}\{[(U_1+U_2)k^2+2(F_1U_2+F_2U_1)]k^2-\beta(k^2+F_2)-B(k^2+F_1)\},\end{aligned} \tag{8a}$$

$$\begin{aligned}Q(\mathbf{k})&=\frac{1}{2a(\mathbf{k})}[4a(\mathbf{k})\,c(k)-b^2(\mathbf{k})]^{\frac{1}{2}}\\&=\frac{|k_x|}{2k^2(k^2+F_1+F_2)}\{S^2k^8+2(B-\beta)Sk^6+[(B-\beta)^2+2(BF_1-\beta F_2)S\\&\quad-4F_1F_2S^2]k^4+2(B-\beta)(BF_1-\beta F_2-2F_1F_2S)k^2+(BF_1+\beta F_2)^2\}^{\frac{1}{2}},\end{aligned} \tag{8b}$$

$$S=U_1-U_2 \quad \text{and} \quad \mathbf{k}=(k_x,k_y).$$

$P(\mathbf{k})\pm Q(\mathbf{k})$ is the frequency of the wave with wave vector $\mathbf{k}$. We can show that it reduces to the form in Robinson & McWilliams (1974) and Pedlosky (1970) in the appropriate limits. An inverse Fourier transform of (5) gives

$$\psi_n(\mathbf{x},t)=\int[A_n\,e^{i(P+Q)t}+B_n\,e^{i(P-Q)t}]\,e^{-i\mathbf{k}.\mathbf{x}}d\mathbf{k}, \quad n=1,2, \tag{9}$$

where A_n and B_n are functions of $\mathbf{k}$ to be determined from the initial conditions. From the governing equations, we can show that A_2 and B_2 are related to A_1 and B_1 by

$$\frac{A_2}{A_1} = \frac{k^2+F_1}{F_1} + \frac{k_x(\beta+F_1 S)}{F_1(P+Q-k_x U_1)} \tag{10a}$$

and

$$\frac{B_2}{B_1} = \frac{k^2+F_1}{F_1} + \frac{k_x(\beta+F_1 S)}{F_1(P-Q-k_x U_1)}. \tag{10b}$$

To determine the two unknowns A_1 and B_1, we need two initial conditions, which can be any two of $\psi_1(\mathbf{x},0)$, $\psi_2(\mathbf{x},0)$, $\partial_t\psi_1(\mathbf{x},t)|_{t=0}$, and $\partial_t\psi_2(\mathbf{x},t)|_{t=0}$. For example, if the disturbance is initially barotropic, we choose $\psi_1(\mathbf{x},0) = \psi_2(\mathbf{x},0) = \phi(\mathbf{x})$, and, if it is initially baroclinic, $\psi_1(\mathbf{x},0) = -\psi_2(\mathbf{x},0) = \phi(\mathbf{x})$. In the real ocean, the initial conditions of the eddies are, of course, unknown. Hence no information about the baroclinicity of the eddy field can be obtained from the model except at very great distances (see §4.2). Since we are only interested in the time scale and the general patterns of development of the eddies, which do not depend sensitively on the initial conditions, except perhaps in a neutrally stable shear, we arbitrarily choose

$$\psi_n(\mathbf{x},0) = 0 \quad \text{and} \quad \partial_t\psi_n(\mathbf{x},t)|_{t=0} = \Phi(\mathbf{x}). \tag{11a, b}$$

These two equations apply to either the upper layer or the lower layer but not to both. For definiteness, we let $n = 1$. We find from (9) that

$$A_1 = -B_1 = -i\Phi(\mathbf{k})/2Q(\mathbf{k})$$

and

$$\psi_1(\mathbf{x},t) = \int \Phi(\mathbf{k})\frac{\sin(Qt)}{Q}\cos(Pt-\mathbf{k}.\mathbf{x})\,d\mathbf{k}, \tag{12}$$

where $\Phi(\mathbf{k})$ is the Fourier transform of $\Phi(\mathbf{x})$. $\psi_2(\mathbf{x},t)$ can be obtained by inserting (12) into (3*a*) or (3*b*).

The time evolution of ψ_1 depends critically on the properties of $Q(\mathbf{k})$. It is shown in appendix B that $Q(\mathbf{k})$ is real in the entire real $\mathbf{k}$-plane if

$$-\beta/F_1 < U_1 - U_2 < B/F_2. \tag{13}$$

For parameters satisfying this relation, ψ_1 is bounded for large t and thus stable. Equation (13) is an extension of Pedlosky's (1964) condition for stability to include bottom slope. It also agrees with the result of Gill *et al.* (1974) in the limit of small bottom slope. For $U_1 - U_2$ outside the range of (13), $Q(\mathbf{k})$ is imaginary for k (k is the magnitude of $\mathbf{k}$) between k_a and k_b, the two real roots of $Q = 0$, and real in the remaining area of the $\mathbf{k}$-plane.† The imaginary $Q(\mathbf{k})$ causes $\sin(Qt)$ and thus $\psi_1(\mathbf{x},t)$ to increase exponentially at large t. At the threshold for stability, $U_1 - U_2 = -\beta F_1$, or B/F_2, $k_a = k_b \equiv k_t$. The area of imaginary $Q(\mathbf{k})$ is reduced to a circular line with radius $k = k_t$.

We want to emphasize here that, although a specific $\Phi(\mathbf{k})$ will be used in the numerical computations for $\psi_1(\mathbf{x},t)$ in §5, the general characteristics of the radiation fields to be discussed in the following section are independent of the initial conditions.

† In general, $Q(k^2) = 0$ has four roots in k^2. If we restrict ourselves to a small bottom slope, only two roots are positive.

4. Approximate and asymptotic solutions

4.1. *The near field*

Longuet-Higgins (1965) has shown that in the absence of a mean shear, the radiation field of a point source is confined to a region of dimension of the order $\beta t \times$ (radius of deformation)^2. The two-layer shear system we consider here gives two radii of deformation, i.e. baroclinic and barotropic deformation radii. The former is given by $\lambda_c = (F_1+F_2)^{-\frac{1}{2}}$ and the latter is infinity as a result of the rigid lid assumption of the model. The effects of the shear on the radiation field are expected to be different for shears with differing stability properties. We shall discuss the near field solutions of (9) or (12) for a stable, an unstable, and a neutrally stable shear separately.

(*a*) *Stable shear*, $-\beta/F_1 < U_1-U_2 < B/F_2$. The frequencies $P+Q$ and $P-Q$ are real, and, for $k_x > 0$, are associated with the baroclinic and the barotropic quasi-geostrophic waves respectively. To see this, we evaluate $P \pm Q$ for two special cases. Let $U_1 = U_2 = 0$ and $B = \beta$ in (8*a*) and (8*b*); we find

$$P+Q = -\beta k_x/(k^2+F_1+F_2) \quad \text{for the baroclinic Rossby wave,}$$

$$P-Q = -\beta k_x/k^2 \quad \text{for the barotropic Rossby wave.}$$

In another special case, $H_2 \gg H_1$ and $U_1 = U_2 = 0$, we can show that

$$P+Q = -\beta k_x/(k^2+F_1) \quad \text{for the baroclinic Rossby wave,}$$

$$P-Q = -Bk_x/k^2 \quad \text{for the barotropic Rossby wave and topographic Rossby wave.}$$

For $k_x < 0$, the roles of $P+Q$ and $P-Q$ are exchanged. For the rest of this section, we will be concerned only with the $k_x > 0$ half of the **k**-space, since an extension to the other half is trivial.

The dominant contributions to the integral in (9) come from the neighbourhoods of the stationary points of the phase function $\phi_\pm$ in the **k**-plane defined by

$$\phi_\pm = (P \pm Q)t - \mathbf{k}.\mathbf{x}.$$

In other words, the dominant local wavenumber, $\mathbf{k}_\pm$, at a given $(\mathbf{x}, t)$ is determined by

$$\nabla_k \phi_\pm = 0,$$

where ∇_k is the gradient operator with respect to **k**. The local frequency and group velocity are given by $P(\mathbf{k}_\pm) \pm Q(\mathbf{k}_\pm)$ and $\mathbf{x}/t$ respectively (Whitham 1974). We first consider the baroclinic phase function ϕ_+. ϕ_+ has two stationary points corresponding to a maximum and a minimum for small $|\mathbf{x}|/t$ except on part of the x axis. As $|\mathbf{x}|/t$ increases, the two points move towards each other until they coincide at a critical point. The locus of such critical points defines a closed curve outside of which no wave associated with ϕ_+ exists. Longuet-Higgins' (1965) calculations for a barotropic model show that the boundary of the radiation field is a comet-shaped loop with the tail pointing to the west. In our model, the determination of the boundary in arbitrary directions involves much complicated algebra. Here we will calculate only the limits of the radiation field on the x axis.

For $\mathbf{x} = (x, 0)$, the stationary points lie on the k_x axis, and ϕ_+ can be written in the form

$$\phi_+ = [P(k_x)+Q(k_x)]t - k_x x, \tag{14}$$

where $P(k_x)$ and $Q(k_x)$ are obtained from $P(\mathbf{k})$ and $Q(\mathbf{k})$ by letting $k_y = 0$. For definiteness, we assume $BF_1+\beta F_2 > 0$. A negative $BF_1+\beta F_2$ results in the replacement of $P+Q$ by $P-Q$ in the following calculations. From (8*a*) and (8*b*) we have

$$P+Q \sim \frac{BF_1U_2+\beta F_2U_1-\beta B}{BF_1+\beta F_2}k_x+O(k_x^3) \quad \text{as} \quad k_x\to 0 \tag{15}$$

and

$$P+Q \sim \tfrac{1}{2}(U_1+U_2+|U_1-U_2|)\,k_x \quad \text{as} \quad k_x\to\infty. \tag{16}$$

We now discuss cases (i) $U_1+U_2=0$, $U_1-U_2\neq 0$, and (ii) $U_1+U_2\neq 0$, $U_1-U_2=0$, separately in order to see the effects of the shear and the average mean current. In case (i), $P+Q$ as a function of k_x has negative values for small k_x. As k_x increases, it reaches a minimum before it rises again at large k_x. We define new variables ξ and η by

$$\xi = (F_1+F_2)\,x/\beta t \quad \text{and} \quad \eta = (F_1+F_2)\,y/\beta t.$$

Let ξ_0 be the value of ξ at which

$$\phi_+ = \partial\phi_+/\partial k_x = 0, \quad k_x\to\infty.$$

From (16), we find

$$\xi_0 = \frac{F_1+F_2}{2\beta}|U_1-U_2|.$$

For ξ slightly greater than ξ_0, ϕ_+ has two stationary points corresponding to tw wave systems. As ξ increases further, the two points move towards each other until they coincide at $\xi=\xi_+$. Beyond ξ_+, there is no stationary point and hence no radiation. For $\xi<\xi_0$, there is one stationary point between ξ_- and ξ_0 where ξ_- is given by

$$\partial\phi_+/\partial k_x = 0, \quad k_x\to 0.$$

From (15), we have

$$\xi_- = \frac{(F_1+F_2)\,(BF_1U_2+\beta F_2U_1-\beta B)}{\beta(BF_1+\beta F_2)}.$$

To summarize:

$$\xi_- < \xi < \xi_0, \quad \text{one stationary point;}$$

$$\xi_0 < \xi < \xi_+, \quad \text{two stationary points;}$$

$$\xi < \xi_- \quad \text{or} \quad \xi > \xi_+, \quad \text{no stationary point.}$$

The radiation field exists on the ξ axis between ξ_- and ξ_+. In the x-space, the two boundary points expand outward at constant speeds. We note that analogous to Longuet-Higgins' results (1965) the boundary of the radiation field for ϕ_+ is a closed loop in the (ξ,η) space, which intercepts the ξ axis at ξ_- and ξ_+. There are two wave systems within the loop except along the ξ axis between ξ_- and ξ_0, which is the limiting line of one of the wave systems. Thus the western boundary of the two-wave region is ξ_- and not ξ_0. Figure 2 shows ξ_0 and $\xi_\pm$ as a function of U_1-U_2. The following set of scales and parameters has been used in all the numerical calculations in this paper:

$$L = (g_r H_1)^{\frac{1}{2}}/f_0 = 50\,\text{km}, \quad U_0 = 1\,\text{cm s}^{-1}, \quad T = L/U_0 = 58\,\text{days},$$

$$F_1 = 1, \quad F_2 = H_1/H_2 = 0{\cdot}18 \quad \text{and} \quad \beta = B = 5.$$

For $U_1-U_2=0$, Longuet-Higgins' values of $(\xi_-,\ \xi_0,\ \xi_+) = (-1, 0, 0{\cdot}125)$ are recovered. The shears significantly change the expansion speed of the boundary. For

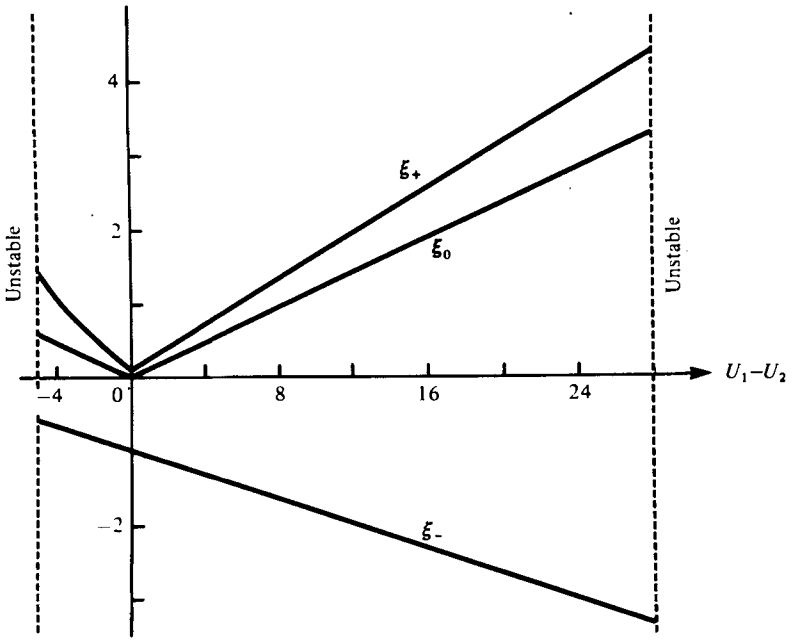

FIGURE 2. The eastern boundary, ξ_+, and the western boundary, ξ_-, of the radiation field associated with $P+Q$ as functions of the mean shear. ξ_0 is the point dividing regions of two waves and one wave.

example, in dimensional units, the expansion speed of the eastern boundary increases from 0·46 km/day for no shear to 5·86 km/day for a shear of + 10 cm s^{-1}.

In case (ii), a similar argument as for case (i) can be used to find ξ_0 and $\xi_\pm$. In the special case of no bottom slope, the algebra is relatively simple and we can show that

$$\xi_0 = \frac{(F_1+F_2)}{\beta}\tfrac{1}{2}(U_1+U_2), \quad \xi_- = -1+\xi_0, \quad \xi_+ = 0{\cdot}125+\xi_0.$$

Thus the average mean current causes a translational movement with a velocity of $\frac{1}{2}(U_1+U_2)$ for the entire wave system.

The barotropic part of ψ_n is governed by $P-Q$, which behaves like

$$P-Q \sim -(\beta F_2+BF_1)/(F_1+F_2)\,k_x \quad \text{as} \quad k_x \to 0$$

and

$$P-Q \sim \tfrac{1}{2}(U_1+U_2-|U_1-U_2|)\,k_x \quad \text{as} \quad k_x \to \infty.$$

Similar to ϕ_+, the number of stationary points of ϕ_- is determined by its behaviour at $k_x \to \infty$. We can show that

$$\xi \leqslant \xi_0, \quad \text{no stationary point;}$$

$$\xi > \xi_0, \quad \text{one stationary point,}$$

where $\xi_0 = [\frac{1}{2}(F_1+F_2)/\beta]\,(U_1+U_2-|U_1-U_2|)$. The difference in the number of stationary points between ϕ_+ and ϕ_- originates from the difference in behaviour near the origin. $P-Q$ has a k_x^{-1} singularity at the origin and is a monotonically increasing function of k_x for $\xi = \xi_0$ while $P+Q \propto k_x$ near the origin. Since there is always one stationary point in the ξ, η space except along the line $\eta = 0, \xi < \xi_0$, which is the limiting line of the wave

system, the wave field associated with $P-Q$ has no boundary. Inside the boundary for $P+Q$, both the barotropic and the baroclinic waves exist. Outside the boundary, only barotropic waves are present.

The total field at a given $(\mathbf{x}, t)$ can be evaluated by the method of stationary phase (Whitham 1974), which gives

$$\psi_n(\mathbf{x},t) = \frac{2\pi}{t}\left(\sum_j \frac{A_n(\mathbf{k}_{+j})}{D_+(\mathbf{k}_{+j})}\exp\{i[\phi_+(\mathbf{k}_{+j}) \pm \tfrac{1}{4}\pi]\} + \sum_j \frac{B_n(\mathbf{k}_{-j})}{D_-(\mathbf{k}_{-j})}\exp\{i[\phi_-(\mathbf{k}_{-j}) \pm \tfrac{1}{4}\pi]\right), \quad (17)$$

where
$$D_\pm(\mathbf{k}) = \frac{\partial^2\phi_\pm}{\partial k_x^2}\frac{\partial^2\phi_\pm}{\partial k_y^2} - \left(\frac{\partial^2\phi_\pm}{\partial k_x\,\partial k_y}\right)^2.$$

The signs in the phase factor $e^{\pm i\pi/4}$ correspond to the signatures of $D_\pm$. $\mathbf{k}_{\pm j}$ is the jth stationary point of $\phi_\pm(\mathbf{k})$. The summations are over all stationary points in the $\mathbf{k}$-space. Equation (17) is not strictly valid in the neighbourhood of the radiation boundary for $\phi_+(\mathbf{k})$. A more accurate representation in the neighbourhood of the boundary is an Airy function which is wave-like inside the boundary and exponential outside the boundary.

(*b*) *Unstable shear, $U_1-U_2 < -\beta/F_2$ or $U_1-U_2 > B/F_2$.* For the discussion of this case, it is more convenient to use (12), which corresponds to the initial conditions (11*a*) and (11*b*). If we were to use a non-vanishing $\psi_1(\mathbf{x}, 0)$ instead of (11*a*), the only change to the solution would be an addition of a term to (12) of the form

$$\int \Phi_1(\mathbf{k})\cos(Qt)\cos(Pt-\mathbf{k}.\mathbf{x})\,d\mathbf{k},$$

where $\Phi_1(\mathbf{k})$ is the Fourier transform of $\psi_1(\mathbf{x}, 0)$. The following calculations can be applied to this additional term with only minor changes.

For $\mathbf{k}$ in the imaginary region of $Q(\mathbf{k})$, i.e. $k_a < k < k_b$,

$$\sin Qt \simeq \tfrac{1}{2}e^{|Q|t}, \quad |Q|t \gg 1. \quad (18)$$

Hence the annular area defined by $k_a < k < k_b$ in the $\mathbf{k}$-space gives the largest contribution to (12) for large t. Let $\mathbf{k}_0$ be the position of the maximum of $|Q(\mathbf{k})|$ within the annular space. Since $Q(\mathbf{k})$ is of the form

$$Q(\mathbf{k}) = |\cos\theta| \times (\text{function of } k), \quad (19)$$

where θ is the angle of $\mathbf{k}$, the maxima always occur in pairs on the k_x axis. We expand $P(\mathbf{k})t-\mathbf{k}.\mathbf{x}$ and $|Q(\mathbf{k})|$ about $\mathbf{k}_0$:

$$P(\mathbf{k})t-\mathbf{k}.\mathbf{x} = P(k_0)t - k_0 x + (P_{0x}t-x)(k_x-k_0) - k_y y + \ldots, \quad (20)$$

$$|Q(\mathbf{k})| = Q_0 + \tfrac{1}{2}[Q_{xx0}(k_x-k_0)^2 + Q_{yy0}k_y^2] + \ldots, \quad (21)$$

where
$$\mathbf{k} = (k_0, 0), \quad Q_0 = |Q(\mathbf{k}_0)|, \quad P_{0x} = \left.\frac{\partial P}{\partial k_x}\right|_{\mathbf{k}=\mathbf{k}_0}, \quad Q_{xx0} = \left.\frac{\partial^2|Q|}{\partial k_x^2}\right|_{\mathbf{k}=\mathbf{k}_0}$$

and
$$Q_{yy0} = \left.\frac{\partial^2|Q|}{\partial k_y^2}\right|_{\mathbf{k}=\mathbf{k}_0}.$$

Substituting (18) to (21) into (12) and evaluating the other factors in the integral at k_0, we have after some manipulation

$$\psi_1(\mathbf{x},t) = \pi\frac{\Phi(\mathbf{k}_0)+\Phi(-\mathbf{k}_0)}{Q_0(Q_{xx0}Q_{yy0})^{\frac{1}{2}}t}\exp(Q_0 t)\cos[P(\mathbf{k}_0)t-kx] \times \exp\left(-\frac{1}{2}\left[\frac{(P_{0x}t-x)^2}{Q_{xx0}t} + \frac{y^2}{Q_{yy0}t}\right]\right), \quad Q_0 t \gg 1. \quad (22)$$

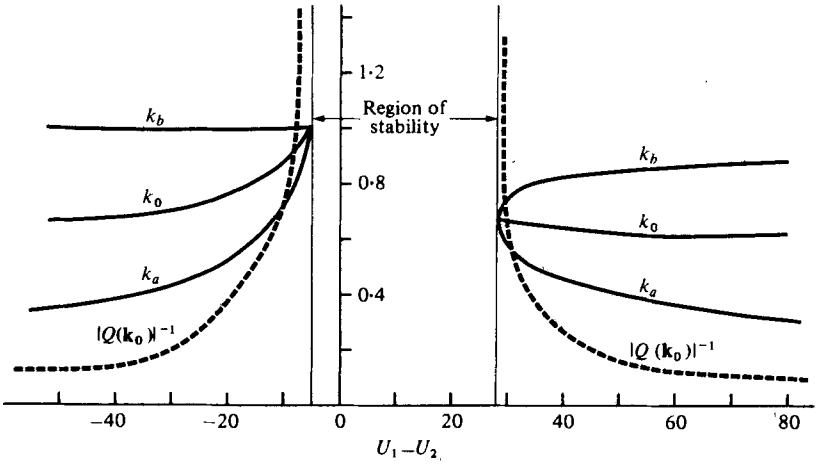

FIGURE 3. The wavenumber, k_0, and the e-folding time, $|Q(\mathbf{k}_0)|^{-1}$, of the most unstable waves against the mean shear. k_a and k_b are the two limits between which $Q(\mathbf{k})$ is imaginary.

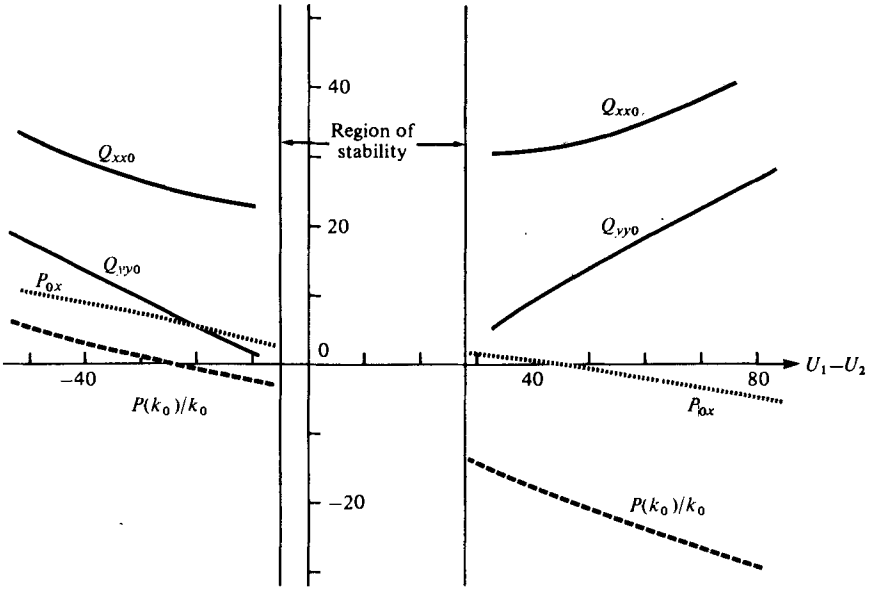

FIGURE 4. Q_{xx0} and Q_{yy0}, the two quantities related to the e-folding distances in the x and y directions of an unstable wave packet by $x = (2Q_{xx0}\,t)^{\frac{1}{2}}$ and $y = (2Q_{yy0}\,t)^{\frac{1}{2}}$ respectively, are plotted against the mean shear. P_{0x} is the velocity of the wave package. $P(k_0)/k_0$ is the phase velocity of the waves in the wave packet.

Equation (22) represents an exponentially growing wave packet which travels in the east–west direction at a velocity of P_{0x}. The dimensions of the wave packet increase as $t^{\frac{1}{2}}$. The e-folding distances in the x and the y directions from the centre are $(2Q_{xx0}\,t)^{\frac{1}{2}}$ and $(2Q_{yy0}\,t)^{\frac{1}{2}}$, respectively. The mathematical problem and the method we used to derive (22) are very similar to Benjamin's (1961) spot development in an unstable film of liquid flowing down an inclined plane.

For $t \gg (2Q_{xx0})^{-1}$, $(2Q_{yy0})^{-1}$, (22) becomes a growing plane wave with an e-folding

time of Q_0^{-1} and a phase velocity of $P(\mathbf{k}_0)/k_0$. This is the stage at which the conventional single wave analysis of baroclinic instability applies.

Figure 3 shows Q_0^{-1}, k_0, k_a, and k_b as functions of U_1-U_2. k_0 is finite and slowly varying with the shear in the entire range of the unstable shear. The expansion parameters of the wave packet, Q_{xx0} and Q_{yy0}, are plotted against U_1-U_2 in figure 4. Near the thresholds, Q_0 becomes very small and (22) ceases to be a good approximation. To get some idea about the time and spatial scales involved, we take $U_1-U_2=-10$ (10 cm s^{-1} in dimensional units) and $t=3$ (174 days), which give from figure 4 an e-folding distance of $x=11{\cdot}7$ (585 km) and $y=3$ (150 km). The wave packet expands in the east–west direction at a much faster rate than in the north–south direction. In comparison, for a stable shear with the same magnitude, $U_1-U_2=10$, the eastern boundary of the baroclinic radiation field reaches a distance of 1020 km in the same period of time.

The phase velocity $P(k_0)/k_0$ and the velocity of the wave packet P_{0x} are also shown in figure 4 for the special case of $U_1+U_2=0$. We note that the phase and the group velocities are more sensitive to U_1+U_2 than to the shear.

(*c*) *Neutrally stable shear*, $U_1-U_2=-\beta/F_1$ *or* $U_1-U_2=B/F_2$. Without loss of generality, we let U_1-U_2 be equal to one of the thresholds, say B/F_2. From (8*b*) we can show that

$$Q(\mathbf{k})=\frac{|k_x|}{2k^2(k^2+F_1+F_2)}\frac{B}{F_2}|k^4-k_t^4|,$$

where

$$k_t^2=\tfrac{1}{2}F_2[(1+\beta/B)^2+4F_1/F_2]^{\frac{1}{2}}.$$

$Q(\mathbf{k})$ has a discontinuity in the first derivative at $k=k_t$ and hence the method of stationary phase fails. Furthermore, it can be shown that the phase velocity associated with $P\pm Q$ is equal to U_2 for $k\leqslant k_t$, and hence some Fourier components of the initial state become non-dispersive. Consequently, there is no simple analytical form to describe the time development of the perturbation at large t. The field is stable in the sense that no Fourier component can grow exponentially at large t.

A particularly interesting point in this case is the neutrally stable wave, the wave with wavenumber $k=k_t$. The integrand of (12) in the limit of $k\to k_t$ is

$$\bar{\Phi}(\mathbf{k}_t)\,t\cos[P(\mathbf{k}_t)\,t-\mathbf{k}_t.\mathbf{x}].$$

If the disturbance is isotropic initially, $\bar{\Phi}(\mathbf{k}_t)=\bar{\Phi}(k_t)$. The amplitude of this wave is independent of the direction of $\mathbf{k}_t$. Hence a neutrally stable wave has no preferred direction of propagation in contrast to an unstable wave, which tends to align its wave vector with the mean shear. This implies that the eddy field is isotropic if the mean shear is neutrally stable. This result is consistent with Moura & Stone (1976) in which it was shown that the meridional scale of the eddy field was of the order of the baroclinic deformation radius, the same as the zonal scale, if the vertical shear is near the threshold for stability. The natural selection of such a meridional length scale is not because the neutrally stable wave is the most unstable wave (its growth rate is zero), but because of the isotropic character of the wave.

4.2. *The far field*

Outside the boundary of the baroclinic radiation field or the region of the unstable wave packet, only waves with frequency $P-Q$ exist. The motion there is independent

of the stability of the shear and is governed by the dispersion relation of the barotropic quasi-geostrophic waves. Since, at great distances, the local approximation for topography is no longer valid, we shall only consider the case without bottom slope in this section.

The properties of $P-Q$ have been discussed in the last section. It was shown that, for a given $\mathbf{x}/t$, there was only one stationary point, $\mathbf{k}_-$, for ϕ_- in the $\mathbf{k}$-space except on part of the x axis. In general, k_- (the magnitude of $\mathbf{k}_-$) decreases with increasing $\mathbf{x}/t$. In the limit $\mathbf{x}/t \to \infty$, we can show that

$$k_- = \left(\frac{F_1+F_2}{\xi}\right)^{\frac{1}{2}}, \quad \theta_{k_-} = 0 \quad \text{for} \quad \eta = 0$$

and

$$k_- = \left(\frac{F_1+F_2}{\eta}\right)^{\frac{1}{2}}, \quad \theta_{k_-} = \frac{\pi}{4} \quad \text{for} \quad \xi = 0,$$

where θ_{k_-} is the direction of $\mathbf{k}_-$.

For small $\mathbf{k}_-$, the frequency is given by

$$P-Q = -\frac{\beta k_- \cos\theta_{k_-}}{k_-^2} + \frac{F_1 U_2 + F_2 U_1}{F_1+F_2} k_- + O(k_-^3).$$

The second term is the Doppler shift due to the mean currents. Thus the far field consists mainly of long barotropic Rossby waves with Doppler shifts in their frequencies.

To examine the relative motions of the upper and the lower layers, we calculate ψ_2/ψ_1 from (17) and (10*b*)

$$\psi_2(\mathbf{x},t)/\psi_1(\mathbf{x},t) = B_2(\mathbf{k}_-)/B_1(\mathbf{k}_-).$$

In the absence of the mean currents, $B_2/B_1 = 1$, indicating a pure barotropic motion. With the mean currents, this ratio can be either greater or smaller than 1 depending on the value of $U_1 - U_2$. To see this, we expand B_2/B_1 in powers of k_-:

$$\frac{B_2}{B_1} = 1 + \left(\frac{1}{F_2} - \frac{1}{F_1} - \frac{U_1-U_2}{\beta}\right) k_-^2 + O(k_-^4).$$

Since k_- decreases with distance, the motions become more barotropic as the distance from the source increases.

Numerical values of $\mathbf{k}_-$, $P-Q$, and B_2/B_1 for the east–west ($\eta = 0$) and the north–south ($\xi = 0$) directions are plotted in figures 5 and 6 for four different shears. The curves for the east–west direction start at $\xi = \xi_0$, and for both directions the

$$U_1 - U_2 = -10$$

case is unstable and has no stationary $\mathbf{k}_-$ with a magnitude greater than $k_a = 0{\cdot}72$. The most significant feature of these figures is that k_-, the local wave number, for different mean shears converges rapidly to asymptotic values as $\mathbf{x}/t$ increases, especially in the north–south direction. This means that in the ocean interior the length scales are independent of the local mean currents. The frequency and the amplitude ratio, on the other hand, are more sensitive to the mean currents but the trends towards barotropic motions at great distances are definite. Strictly speaking, the model is not valid for

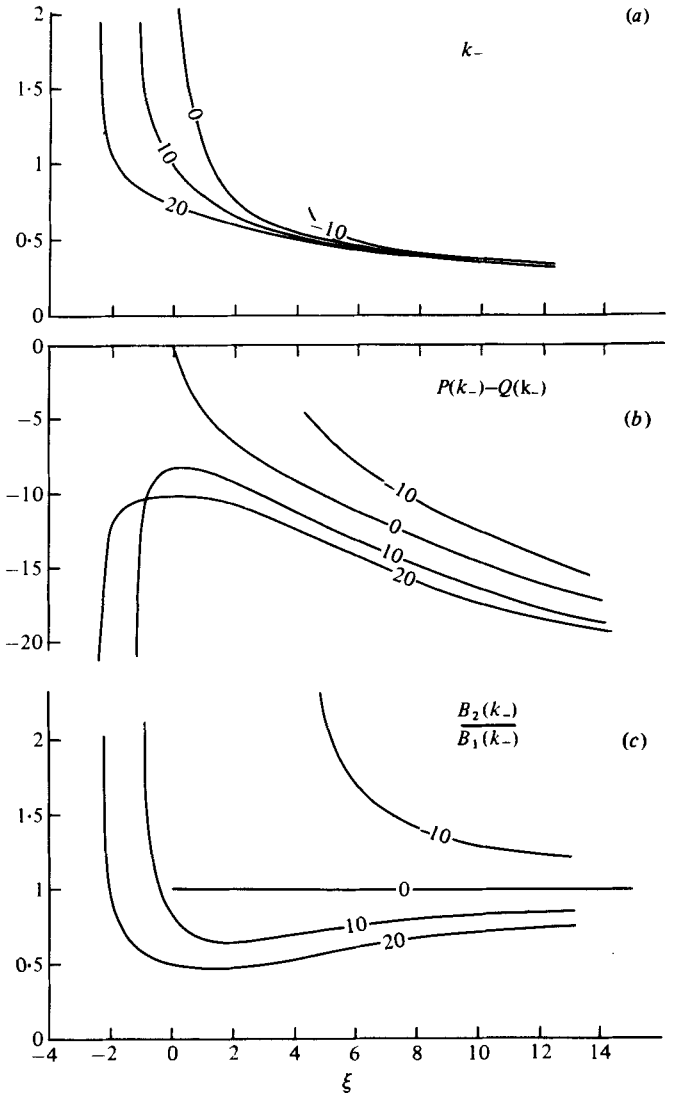

FIGURE 5. (*a*) The stationary wavenumber, $\mathbf{k}_-$, (*b*) the frequency $P-Q$, and (*c*) the amplitude ratio between the two layers, B_2/B_1, for ϕ_- in the east–west direction calculated with four different values of the mean shear, $U_1-U_2 = 0$, 20 and ± 10. $U_1-U_2 = -10$ is unstable and hence ϕ_- has no stationary point for $k > k_a = 0{\cdot}72$. The numbers on the curves denote the values of U_1-U_2. $U_1+U_2 = 0$ is used for all computations.

discussing the far field in an ocean with variable mean currents. However, the relative insensitivity of the far field to the mean currents provides *a posteriori* justification for the use of uniform mean currents to study the gross features of the ocean interior. The results in figures 5 and 6 can be viewed as upper limits of the effect of the mean currents. In a y-dependent shear flow, the local wavenumbers are not expected to deviate much from the asymptotic values. The frequency and the amplitude ratio are probably dependent on some integrals of the mean currents in the WKB sense if the spatial scale of the mean currents is much greater than the wavelengths. Regardless of the

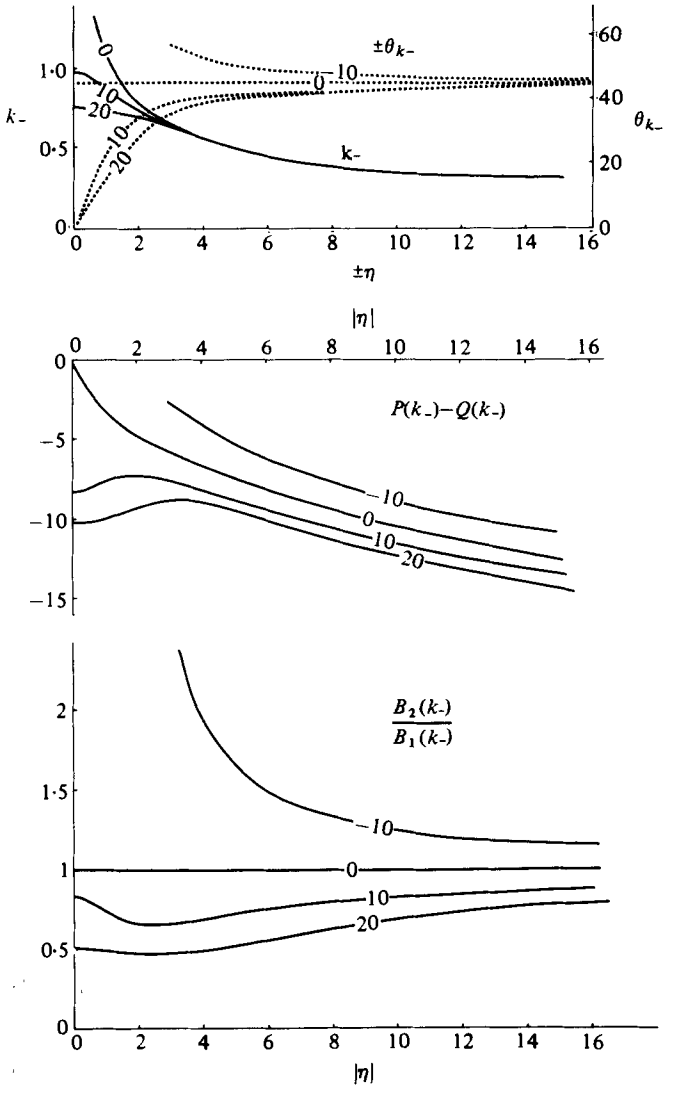

FIGURE 6. The same as figure 5 except that the direction is north–south. The curve for k_- for $U_1 - U_2 = -10$ almost coincides with that for $U_1 - U_2 = 10$ and hence is not shown.

detailed structure of the mean currents, their effects on the wave field will become weaker as the distance increases since the asymptotic forms for $\mathbf{k}_-$, $P-Q$, and B_2/B_1 are all independent of the mean currents.

5. Transient motions

The evolution of $\psi_1(\mathbf{x}, t)$ can be computed numerically from (12) for any given $\Phi(\mathbf{k})$. Since the asymptotic forms are independent of the initial conditions, its specification is not crucial except for very small t, and perhaps for a neutrally stable shear. We choose

$$\Phi(k) = (k^2 + F_1 + F_2)^{-1}. \tag{23}$$

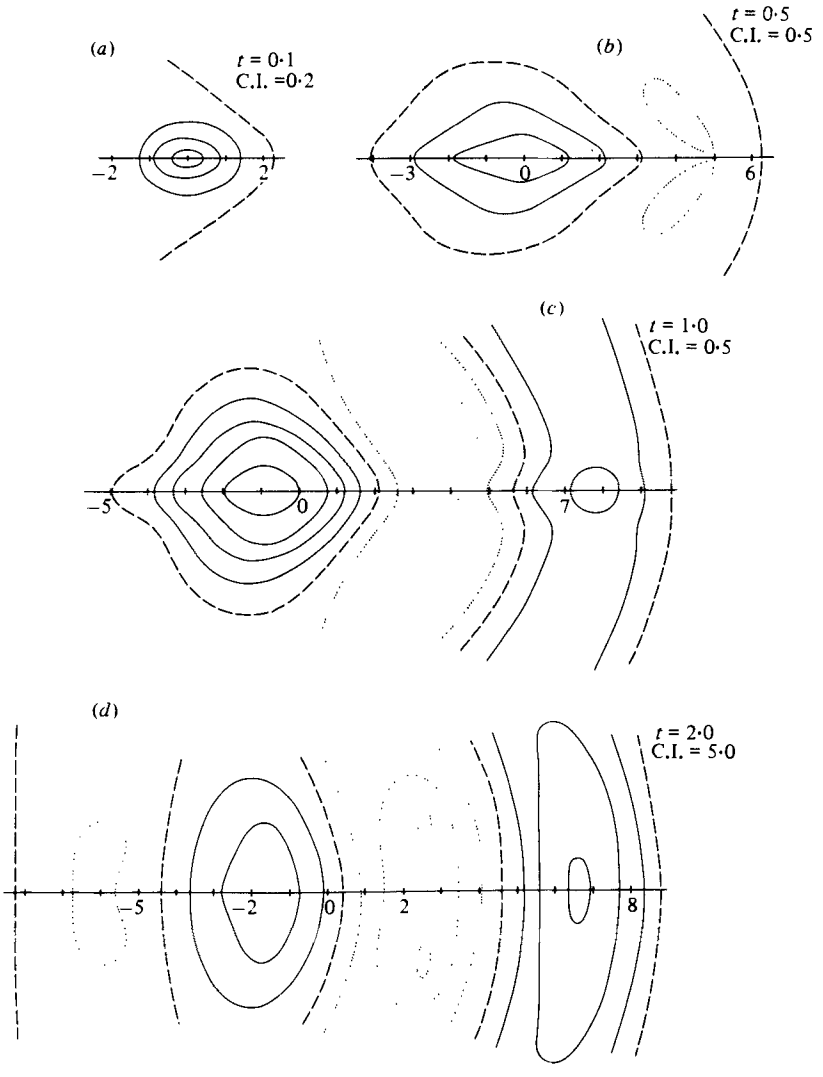

FIGURE 7. Time sequence of ψ_1 for an unstable mean shear, $U_1 - U_2 = -20$, $U_1 + U_2 = 0$. C.I. stands for contour interval; ——, positive value of ψ_1; ..., negative value of ψ_1; – – –, $\psi_1 = 0$. Each division on the x axis represents one non-dimensional unit.

This gives

$$\psi_1(\mathbf{x}, t) \overset{t \to 0}{=} t \int \tilde{\Phi}(\mathbf{k}) \cos(\mathbf{k}.\mathbf{x})\, d\mathbf{k} = 2\pi t\, K_0[(F_1 + F_2)^{\frac{1}{2}} |\mathbf{x}|], \tag{24}$$

where K_0 is the modified Bessel function of the second kind of order 0. It is shown in appendix C that $\psi_1(\mathbf{x}, t)$ as given by (24) is the response of a quasi-geostrophic system with a radius of deformation of $(F_1 + F_2)^{-\frac{1}{2}}$ to a δ-function source term in the absence of the β-effect and mean currents.

The calculations involve two-dimensional integrations. A standard method (Simpson's rule) was used to perform the integrations over k and θ. One point worth noting in the calculation is that P and Q behave as k^{-1} near the origin which causes $\sin(Qt)/Q$ to oscillate faster and faster as $k \to 0$. Such an oscillatory behaviour originates from the

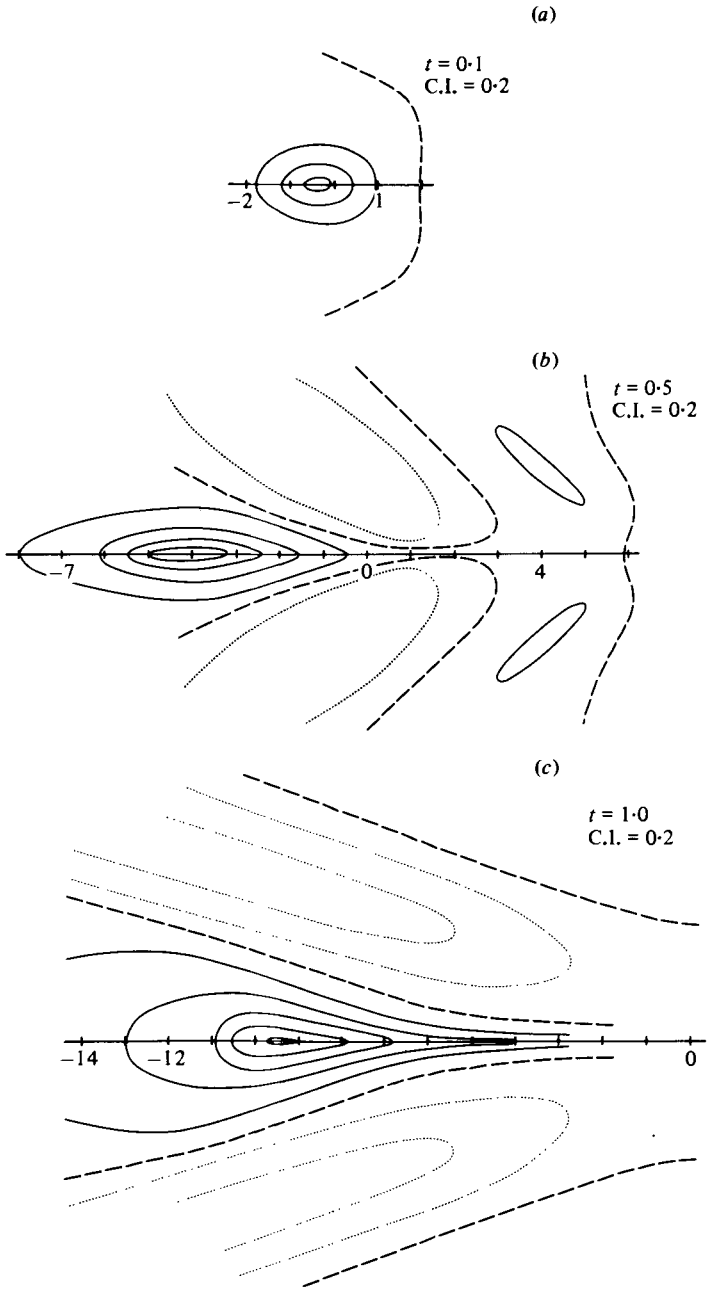

FIGURE 8. Time sequence of ψ_1 for a stable mean shear $U_1 - U_2 = 20$, $U_1 + U_2 = 0$. C.I. stands for contour interval; ——, positive value of ψ_1; ..., negative value of ψ_1; – – –, $\psi_1 = 0$. Each division on the x axis represents one non-dimensional unit.

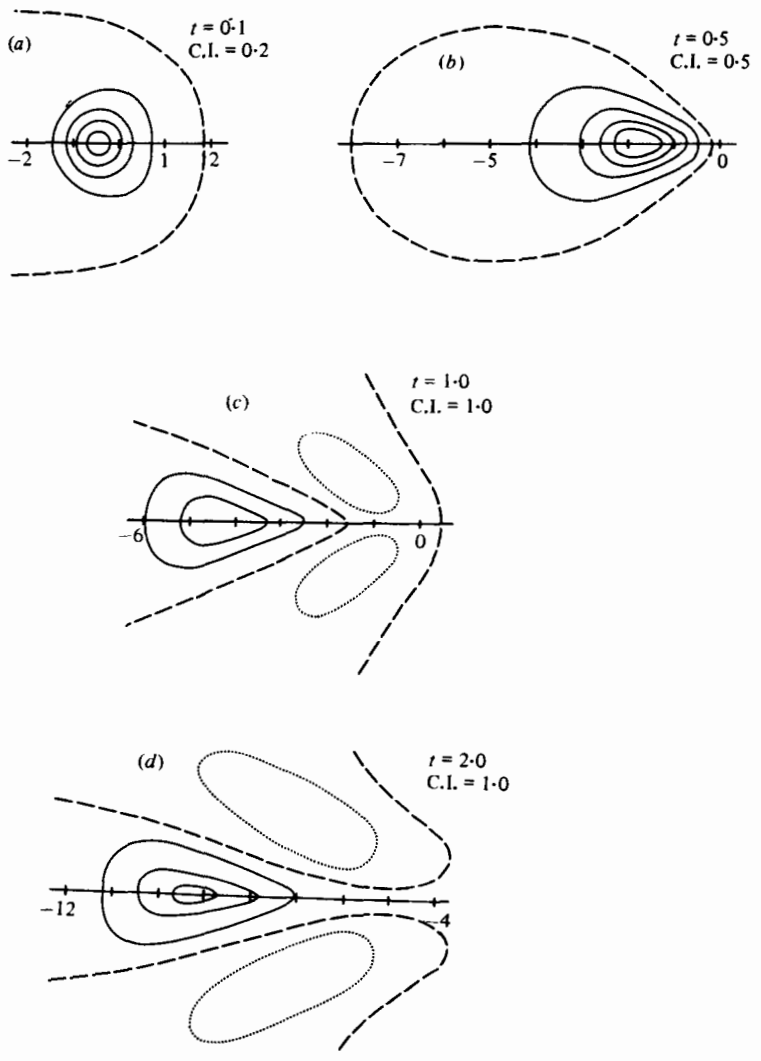

FIGURE 9. Time sequence of ψ_1 for a mean shear at threshold, $U_1 - U_2 = 5$, $U_2 = 0$. C.I. stands for contour interval; ——, positive value of ψ_1; ..., negative value of ψ_1; – – –, $\psi_1 = 0$. Each division on the x axis represents one non-dimensional unit.

fact that we have assumed an infinite barotropic deformation radius in this model. We can show that the contributions from the neighbourhood of the origin are finite and only affect ψ_1 at very large **x**. Our numerical computations are restricted to small **x**.

The scales and parameters used in the numerical calculations are the same as before. The two thresholds of the shear are -5 and 28. Figure 7 shows the time sequence of ψ_1 for $U_1 = -10$, $U_2 = 10$ corresponding to an unstable shear. The centre of the main eddy moves westwards approximately at the phase velocity of the wave k_0, which is, from figure 4, about -1. The β-effect causes an asymmetry in the east–west direction. This asymmetry becomes weaker as t increases. Figure 8 illustrates a stable case with $U_1 = 10$, $U_2 = -10$. The westward movement of the wave system is more sensitive to $|U_1 - U_2|$ than in the unstable case. This is due to the fact that the dispersion of the

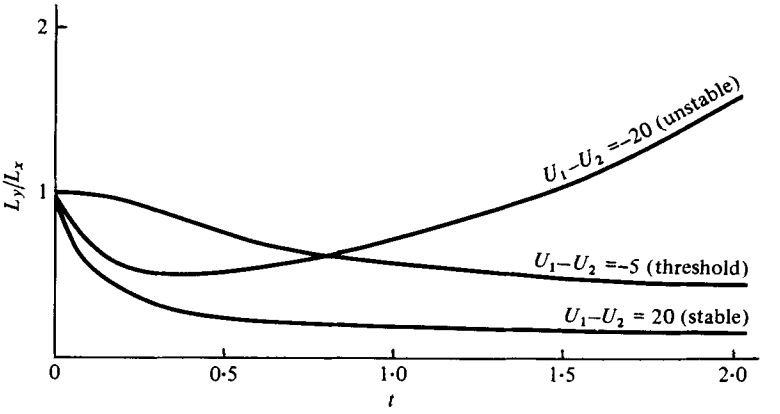

FIGURE 10. The ratio of the meridional length scale L_y to the zonal length scale L_x as a function of time. The length scale is defined as the distance over which the value of the stream function drops to half of the maximum value.

stable waves depends on Q, which is a function of $|U_1 - U_2|$, as well as on P. The wave patterns are somewhat similar to those in Longuet-Higgins (1965) and Rhines (1977) but, owing to the shear, the streamlines in figure 8 are more stretched along the zonal axis. Figure 9 shows a threshold case with $U_1 = -5$, $U_2 = 0$. The main eddy has a slight elongation in the east–west direction, and its shape changes much more slowly than either the stable or the unstable case.

To compare the spatial structure of the three cases, we plot the ratio of the meridional (y direction) scale, L_y, to the zonal (x direction) scale, L_x, against time in figure 10. The scales are defined as the distances over which the values of the stream functions drop to half of their maximum values. At $t = 0$, the ratios are 1, corresponding to an isotropic initial state. As t increases, the ratio for the stable case decreases rapidly as a result of wave dispersion and streamline stretching by the mean shear. The unstable curve drops from 1 to a minimum of about 0·6. As t increases towards and beyond 1, the process of energy conversion starts and accelerates. The effect of baroclinic instability overcomes that of wave dispersion, and the eddy becomes more and more elongated in the meridional direction. In the threshold case, the eddy is isotropic up to about $t \sim 0{\cdot}2$, then slowly changes its shape with the major axis aligned with the mean shear.

Except for the stable case, the isotropy of the eddies is maintained by the combined effects of wave dispersion and baroclinic instability for a considerable period of time, $t \sim 1{\cdot}5$.

6. Summary and discussion

We have solved the initial value problem for eddies in a two-layer zonal shear flow. The solution indicates that two wave regimes in the $\mathbf{x}/t$ plane exist. For a small $\mathbf{x}/t$, the properties of the radiation field depend on the stability of the shear. If the shear flow is baroclinically stable, the radiation field associated with the baroclinic waves is confined to a region around the initial disturbance. The boundary of this region expands linearly with time. The presence of the mean currents significantly increases the expansion rate of the boundary. If the shear flow is baroclinically unstable, a wave

packet with an exponentially growing amplitude is developed at $t \gg 1$. Its dimensions increase as $t^{\frac{1}{2}}$ and its asymptotic form as $t \to \infty$ is an unstable plane wave with a growth rate, a phase speed and a wavenumber identical to those from a conventional analysis of baroclinic instability.

The transient motion (small $\mathbf{x}$ and t) of an eddy starting from a small initial isotropic disturbance is studied by numerically computing the solution of the initial value problem. The patterns of the transient development are determined by the mean shear. In an unstable shear flow, the eddy is roughly isotropic during the entire transient period due to the combined actions of wave dispersion and baroclinic instability. Wave dispersion alone will rapidly transform the eddy into an elongated structure with the streamlines mainly in the zonal direction. Such is the case of an eddy in a stable shear flow. In comparison, a fully developed unstable eddy has parallel streamlines in the meridional direction. Our results suggest that the initial development of eddies cannot be neglected in studying the meridional scale of the atmospheric motions.

Outside the radiation boundary and the unstable wave packet, stable barotropic Rossby waves dominate. As the distance from the initial disturbance increases, the motions tend to be more barotropic, and the wavelengths and the frequencies slowly increase. Applied to the mid-Atlantic, these results seem to be consistent with the observations of Lee Dantzler (1976, 1977) who found that the baroclinic eddy energy decreased as the distance from the western and northern boundary currents increased. A barotropic interior is also indicated in the general circulation numerical models. The interior motions in Robinson *et al.* (1977) is predominantly barotropic while near the boundary currents there is more baroclinic energy than barotropic energy. The length scale of the far field in our model is proportional to the square root of the distance to the source. Semtner & Mintz's numerical model (1977) seems to show a trend towards large spatial scale away from the boundary currents. In the real ocean, a square root variation with distance is probably too weak to be detected. Reflexions from the iregular coastline can result in shorter length scales and complicate the spatial structure.

The far-field solution is not sensitive to change of the magnitude of the mean shear. The main effect of the mean shear is to introduce a Doppler shift in the frequencies. This implies that the interior motions do not depend on the local mean current. The magnitude of the mid-ocean eddy field is determined mainly by the eddy energy generated in the Gulf Stream region. This is in contrast to the result of Pedlosky's (1977) model of a plane-wave source along a latitude line, in which he predicted that the ability of the interior to transmit radiated energy and the vertical structure of the eddy field in mid-ocean are dependent on the velocity and the stability of the local current. The difference in the results arises from the fact that different boundary conditions have been imposed on the equations. The situation in the real ocean is of course much more complicated. The Gulf-Stream-generated eddies as a source is neither in the form of a localized disturbance or in the form of an infinite plane wave, but is probably a combination of the two. Our calculations demonstrate how sensitive the results of a dynamical model are to the way the mathematical problem is posed. Inclusion of the oceanic boundary in the model may help to reduce the discrepancy, but to solve the problem presents a formidable task.

Finally, we apply the model to study certain aspects of the oceanic response to wind systems. The near-field solution indicates that baroclinic waves generated by the wind

are dispersed away from the area of direct wind forcing. The effect of the mean shear is to increase the speed of the dispersion. Thus the energy from the wind is more quickly distributed in a fast current than in a slow current. The barotropic waves radiate outward at infinite speed, a result of the rigid lid assumption of the model. Consequently, at a distance from a storm, we expect to observe barotropic waves arriving before baroclinic waves. The magnitude of the waves can be fixed if a source term is included in the equations of motion. The expansion speed of the radiation field is, however, independent of the forcing term, since it is determined by the mean shear and the dispersion relations of the Rossby waves alone.

Appendix A

We write (3*a*) and (3*b*) in operator forms:

$$\mathscr{L}_{11}\psi_1+\mathscr{L}_{12}\psi_2 = 0 \tag{A 1}$$

and

$$\mathscr{L}_{21}\psi_1+\mathscr{L}_{22}\psi_2 = 0. \tag{A 2}$$

Eliminating one of the dependent variables from (A 1) and (A 2), we have

$$\mathscr{L}\psi_n = 0, \quad n = 1, 2,$$

where

$$\begin{aligned}\mathscr{L} &= \mathscr{L}_{11}\mathscr{L}_{22}-\mathscr{L}_{12}\mathscr{L}_{21}\\ &= \nabla^2[\nabla^2-(F_1+F_2)]\,\partial_t^2+\nabla^2[(U_1+U_2)\nabla^2-2(F_1U_2+F_2U_1)]\,\partial_{xt}\\ &\quad+\nabla^2[U_1U_2\nabla^2-(F_1U_2^2+F_2U_1^2)]\,\partial_x^2\\ &\quad+\beta([\nabla^2-F_2)\,\partial_{xt}+(U_2\nabla^2-U_1F_2)\,\partial_x^2]+B[(\nabla^2-F_1)\,\partial_{xt}\\ &\qquad+(U_1\nabla^2-U_2F_1)\,\partial_x^2]+B\beta\,\partial_x^2.\end{aligned}$$

Appendix B

We show that $Q(\mathbf{k})$ is real for $-\beta/F_1 < S < B/F_2$. The reality of $Q(\mathbf{k})$ is determined by the quantity in the bracket of (8*b*), a function of k^2. Let

$$\begin{aligned}q(k^2) &= S^2k^8+2(B-\beta)Sk^6+[(B-\beta)^2+2(BF_1-\beta F_2)S-4F_1F_2S^2]k^4\\ &\quad+2(B-\beta)(BF_1-\beta F_2-2F_1F_2S)k^2+(BF_1+\beta F_2)^2,\end{aligned} \tag{B 1}$$

$q(k^2)$ is positive if the minimum of $q(k^2)$ is zero or positive. The positions of the extrema are given by

$$\partial q(k^2)/\partial k^2 = 0, \tag{B 2}$$

which is a cubic equation in k^2 and has three solutions corresponding to the one maximum and the two minima of $q(k^2)$:

$$\begin{aligned}k^2_{\max} &= -\frac{B-\beta}{2S};\\ k^2_{\min} &= -\frac{B-\beta}{2S}\pm\frac{1}{2|S|}[(B-\beta)^2-4(F_1B-F_2\beta)S+8F_1F_2S^2]^{\frac{1}{2}}.\end{aligned} \tag{B 3}$$

Substituting (B 3) into (B 1), we have

$$q(k_{\min}^2) = -4F_1F_2^2(S-B/F_2)(S+\beta/F_1).$$

Thus

$$q(k_{\min}^2)\begin{cases}\geqslant 0, & -\beta/F_1 \leqslant S \leqslant \beta/F_2,\\ < 0, & S > B/F_2 \quad \text{or} \quad S < -\beta/F_1.\end{cases}$$

Appendix C

The motion of a linear quasi-geostrophic system with a radius of deformation λ and forcing $\delta(\mathbf{x})\delta(t)$ is governed by (Charney 1956)

$$\partial_t(\nabla^2-\lambda^{-2})\psi = \delta(\mathbf{x})\delta(t), \tag{C 1}$$

with initial condition

$$\psi = 0, \quad t \leqslant 0.$$

Integrating (C 1) over t from 0_- to t gives

$$(\nabla^2-\lambda^{-2})\psi = t\delta(\mathbf{x}). \tag{C 2}$$

The solution of (C 2) by Fourier transform method is

$$\psi = t\int (k^2+\lambda^{-2})^{-1}\exp(i\mathbf{k}.\mathbf{x}) = 2\pi t K_0(|\mathbf{x}|/\lambda).$$

REFERENCES

Benjamin, T. B. 1961 The development of three-dimensional disturbances in an unstable film of liquid flowing down an inclined plane. *J. Fluid Mech.* **10**, 401–419.

Charney, J. G. 1947 The dynamics of long waves in a baroclinic westerly current. *J. Met.* **4**, 135–162.

Charney, J. G. 1956 The generation of oceanic currents by wind. *J. Mar. Res.* **14**, 477–498.

Gill, A. E., Green, J. S. A. & Simmons, A. J. 1974 Energy partition in the large-scale circulation and the production of mid-ocean eddies. *Deep-Sea Res.* **21**, 499–528.

Holland, W. R. & Lin, B. 1975 On the generation of mesoscale eddies and their contribution to the oceanic general circulation. I. A preliminary numerical experiment. *J. Phys. Oceanog.* **5**, 642–657.

Lee Dantzler, H. 1976 Geographic variations in intensity of the North Atlantic and North Pacific oceanic eddy fields. *Deep-Sea Res.* **23**, 783–794.

Lee Dantzler, H. 1977 Potential energy maxima in the tropical and subtropical North Atlantic. *J. Phys. Oceanog.* **7**, 512–519.

Longuet-Higgins, M. S. 1965 The response of a stratified ocean to stationary or moving wind-systems. *Deep-Sea Res.* **12**, 923–973.

Moura, A. D. & Stone, P. H. 1976 The effects of spherical geometry on baroclinic instability. *J. Atmos. Sci.* **33**, 602–616.

Mysak, L. A. & Schott, F. 1977 Evidence of baroclinic instability of the Norwegian Current. *J. Geophys. Res.* **82**, 2087–2095.

Pedlosky, J. 1964 The stability of currents in the atmosphere and the ocean. Part 1. *J. Atmos. Sci.* **21**, 201–219.

Pedlosky, J. 1977 On the radiation of mesoscale energy in the mid-ocean. *Deep-Sea Res.* **24**, 591–600.

Rhines, P. B. 1977 *The Dynamics of Unsteady Currents. The Sea*, vol. 6 (ed. Goldberg *et al.*). New York: Wiley.

Robinson, A. R. & McWilliams, J. C. 1974 The baroclinic instability of the open ocean. *J. Phys. Oceanog.* **4**, 281–294.

ROBINSON, A. R., HARRISON, D. E., MINTZ, Y. & SEMTNER, A. J. 1977 Eddies and the general circulation of an idealized oceanic gyre: a wind and thermally driven primitive equation numerical experiment. *J. Phys. Oceanog.* **7**, 182–207.

SEMTNER, A. J. & MINTZ, Y. 1977 Numerical simulation of the Gulf Stream and mid-ocean eddies. *J. Phys. Oceanog.* **1**, 208–230.

SMITH, P. C. 1976 Baroclinic instability in the Denmark Strait overflow. *J. Phys. Oceanog.* **3**, 355–371.

STERN, M. E. 1975 *Ocean Circulation Physics*, chap. 9. New York: Academic Press.

WHITHAM, G. B. 1974 *Linear and Nonlinear Waves*. New York: Wiley.